5-2014

Consequences of Endogenous Mitochondrial Oxidative Stress in the Heart

Kristin Alisha Koenig
Dominican University of California

https://doi.org/10.33015/dominican.edu/2014.bio.03

Consequences of endogenous mitochondrial oxidative stress in the heart

A thesis submitted to the faculty of

Dominican University of California

&

The Buck Institute for Research on Aging

In partial fulfillment of the requirements

for the degree

Master of Science

in

Biology

By

Kristin Koenig

San Rafael, California

March 2014

Abstract

For many years, it has been proposed that oxidative stress within the mitochondria causes mutations to the mitochondrial genome, resulting in changes in copy number per single cell. Ultimately, this compensatory increase in mtDNA, coupled with an increase in mutations, has been suggested to play a major role in the pathobiology of aging. However, evidence for this phenomenon is somewhat controversial. Importantly, oxidative stress can vary between individual cells; therefore, the overall goal of this project is to determine if oxidative stress causes both an altered copy number for mtDNA in single-cardiomyocytes and develop a methodology for sequencing mtDNA from single cells compared to normal controls.

In this study, the constitutive *Sod2* knockout mouse model was used. All mice were treated daily with the SOD2 mimetic, Euk-189. For the first time, echocardiography was performed on constitutive *Sod2* nullizygous mice. *Sod2* mice were shown to have impaired systolic function, as demonstrated by significantly lower ejection fraction and fractional shortening values. Additionally, these mice show severe cardiac fibrosis and decreased FECH activity in cardiac tissue.

The long-term goal of this project will be to carry out next-generation sequencing on single cardiomyocytes isolated from both *Sod2* knockout and wild-type mice. However, a necessary first step is to develop the methodology for both isolating single cardiomyocytes and to quantitate mtDNA copy number for each single cell. We have been successful in accomplishing both these goals.

The final outcome of these experiments will be to determine mtDNA sequences for multiple mtDNA genomes from single cells, and we hypothesize that mice undergoing endogenous oxidative stress will have accumulated more DNA mutations and deletions than wild-type mice. These data will ultimately inform us as to the role of mitochondrial DNA mutations in cardiac dysfunction.

Acknowledgements:

Simon Melov PhD

Brittany Garrett MS

James Flynn PhD

Christopher Zambataro MS

Dan Crooks PhD

Tracey Rouault PhD

Table of contents:

Abstract: pg. 3-4
Acknowledgements: pg. 5
Table of Contents: pg. 6
Lists: pg. 7
Abbreviations: pg. 8
Background: pg. 9-19
    Overview
    Aging
    Mitochondrial oxidative stress
    Functional echocardiography
    Single-cell analysis
Materials and methods: pg. 19-28
    Overview
    Genotyping
    Functional echocardiography
    Single-cardiomyocyte isolation
    Single-cardiomyocyte mitochondrial genome enumeration
    Masson's trichrome stain
    Western blot
    Densitometry
    Statistical analysis
Future Studies: 29
Results: pg. 30-42
Discussion: pg. 42-44
Future studies: pg. 44
    mtDNA mutation detection
    Gene expression profiling
References: pg. 45-48

Lists:

Figures:

1. Simplified mechanism of the effects of superoxide production
2. Survival curve of *Sod2* knockout mice treated with various antioxidants
3. Structures of salen manganese complexes
4. Equation for determining mitochondrial genome count
5. Primer design for full mitochondrial genome coverage
6. Genotyping Results
7. SOD2 Western blot
8. Weight chart
9. Functional heart metrics
10. Cardiac fibrosis
11. Aconitase activity
12. ISCU activity
13. Ferrochelatase activity
14. Single-cardiomyocyte mitochondrial genome enumeration
15. Mitochondrial genome enumeration summary

Tables:

1. Genotyping Reaction: PCR
2. Digestion buffer solutions
3. BioMark Digital PCR Analysis Sample pre-mix

Abbreviations:

EF – ejection fraction

mAco - aconitase

mtDNA – mitochondrial DNA

FECH - ferrochelatase

ISCU – iron sulfur cluster assembly enzyme

FS - fractional shortening

KO – knockout

ROS - reactive oxygen species

Sod2 – super oxide dismutase (mitochondrial) gene

SOD2- super oxide dismutase (mitochondrial) enzyme

WT- wild type

Background:

Overview

Heart disease is a major age-related disorder, and defining the underlying molecular mechanisms that drive this disorder is becoming an economic necessity. Work in the heart is primarily performed by one of the main cell types comprising this organ, the cardiomyocyte. During this process of carrying out work, oxidative stress is produced within mitochondria that “power” the cardiomyocyte.

Murine models play an important role in translational research and give new insights into the mechanisms that drive disease. Mice are widely used because of the relative ease of genetic manipulations, the relatedness to human physiology, and they are relatively inexpensive to house and maintain.

Mitochondrial Oxidative Stress

The heart has substantial ATP requirements, and most of the ATP is derived from mitochondrial oxidative phosphorylation. Oxidative phosphorylation involves several electron transfers along the respiratory chain and results in the reduction of O_2 to H_2O and ATP production (Figure 1). While the exact site(s) and levels of reactive oxygen species (ROS) are still under active investigation, previous reports have indicated that around 0.4-4% of all oxygen used can be converted into superoxide (O_2^-) free radicals (Turrens & Boveris, 1980). Most mitochondrial superoxide is produced from complex 1 and 3 of the respiratory chain (Raha et al., 2000). When electrons are transferred from reducing

equivalents through the respiratory chain, complex 1 generates ROS at rates that may be pathologically relevant (Turrens & Boveris, 1980).

We were interested in understanding how endogenous oxidative stress, within the constitutive *Sod2* knockout mouse model, affects the activity of the ISCU enzyme. Oxidative stress is known to negatively affect the mammalian iron sulfur cluster assembly (ISCU) machinery by destabilizing the ISCU enzyme. Iron-sulfur cluster cofactors are constructed on the scaffolding protein, ISCU (Crooks et al., 2012).

In addition to observing how oxidative stress affects ISCU activity, we were also interested in the effects of oxidative stress on the activity of an iron-sulfur-containing enzyme, ferrochelatase (FECH), which catalyzes the final step in the biosynthesis of heme within the mitochondrion. Heme contains an iron-sulfur group, and behaves as a cofactor of hemoproteins. Heme is crucial in many metabolic processes due to its ability to confer electron transfer and electron transport to numerous enzymes (Crooks et al., 2012).

Figure 1 – Simplified mechanism of the effects of superoxide production

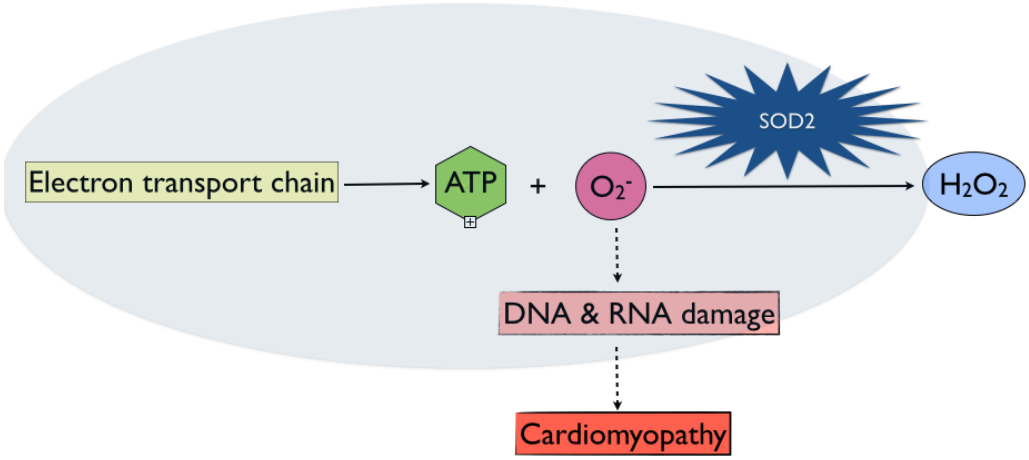

Fig.1. The electron transport chain results in the production of ATP and superoxide (O_2^-). Under normal conditions, SOD2 catalyzes the transformation of superoxide into hydrogen peroxide. However, if there is insufficient SOD2 present, superoxide can damage DNA, RNA, and proteins. Over time, this mitochondrial dysfunction could lead to cardiomyopathy, among other pathologies.

ROS have the potential to oxidize DNA, RNA, proteins and lipids (Figure 1). Eukaryotes have acquired defense mechanisms against the potentially harmful effects of ROS, the most noteworthy of which is the mitochondrial Superoxide dismutase enzyme (SOD2). There are three isoforms of superoxide dismutase: SOD1, SOD2, and SOD3. Cu/Zn SOD1 is localized mainly in the cytosol within a cell, while Cu/Zn SOD3 is located outside of the cell (Sturtz et al., 2001). SOD1 and SOD3 play a role in neutralizing ROS, but their roles are not as critical as that of SOD2 (Li et al., 1995; Sturtz et al., 2001). The *Sod2* gene is located on chromosome 6 for humans and chromosome 17 for mice (Raha et al., 2000). SOD2 is found within the mitochondrial matrix, forms a homotetramer that binds one manganese ion per subunit and has been shown to have a critical role in the catalytic removal of superoxide (Li et al., 1995). SOD2 ultimately converts

harmful superoxide into the less toxic hydrogen peroxide, which has the ability to diffuse across the mitochondrial membrane unlike superoxide. Mice that have been genetically altered to lack *Sod2* on a CD-1 background develop mitochondrial biochemical defects, dilated cardiomyopathy within the first week of life, severe accumulation of fat within the liver, and ultimately a neonatal/embryonic lethal phenotype (Li et al., 1995; Melov et al., 1998).

Sod2 can be genetically inactivated via homologous recombination (Li, et al., 1995). Mice nullizygous for the *Sod2* allele on a CD-1 background (CD1-*Sod2*^{tm1Cje}) have a neonatal lethal phenotype within the first ten days of life (Figure 2; Li et al., 1995; Melov et al., 1998; Melov et al., 2001).

Figure 2 – Survival curves of *Sod2* knockout mice treated with various antioxidants

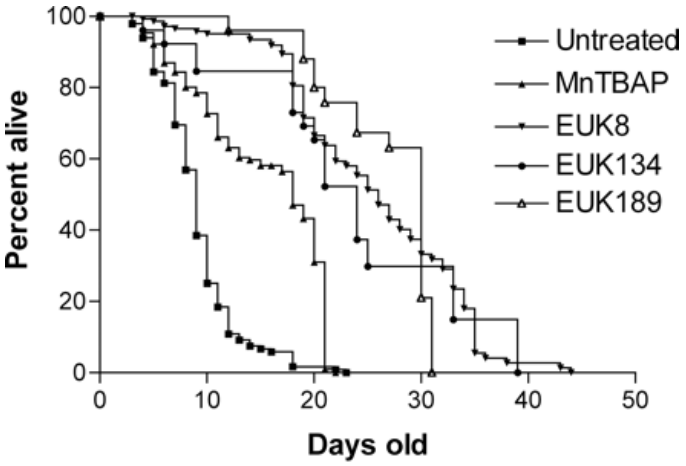

Fig.2. Kaplan-Meier survival analysis of *Sod2* knockout mice treated with various synthetic catalytic antioxidants (Euk-8, Euk-134 and Euk-190) at 30 mg/kg. All antioxidants tested enhanced the survival of these mice. Euk-189 has been used in this study (Melov at al., 2001).

In order to rescue this neonatal lethality, the Melov lab has shown that daily injections of synthetic antioxidants (for example, EUK-189) at 30 mg/kg can extend the lifespan of mice lacking SOD2 by threefold (Figure 2; Melov et al., 2001). EUK-189 is a member of the synthetic salen-manganese Eukarion

complex (Figure 3) and has been shown to mimic activities of the endogenous SOD2 (Doctrow et al., 2002).

Figure 3 - Structures of salen manganese complexes

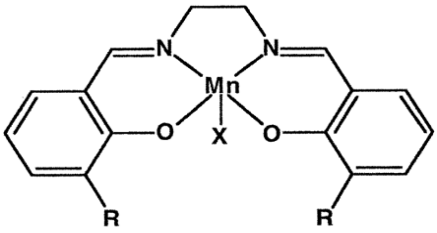

Fig.3. The ring substitutions (*R*) of three salen manganese complexes compounds are shown. In EUK-189, the axial ligand (X) is acetate. This study will use the EUK-189 molecule to rescue the neonatal lethal phenotype of *Sod2* knockout mice (Melov et al., 2001).

EUK-8: R = H
EUK-134: R = OCH_3
EUK-189: R = OCH_2CH_3

Functional Echocardiography

Data from the Framingham Heart Study revealed that the incidence of adults over the age of 65 developing heart failure is 10 per 1,000 population (Lloyd-Jones et al., 2002). Because heart disease is so prevalent, it is critical that the underlying mechanisms involved in the development of this age-related disorder become well understood. Echocardiography is a noninvasive imaging method, with no known side effects, that has proven very useful for the diagnosis of heart disease. By performing high frequency ultrasound imaging of the heart, an investigator can observe in real-time, the function of the heart in a number of different respects.

Single-cell analysis

mtDNA enunumeration and ultimately mtDNA sequencing will be carried out via a combination of nanofluidic PCR and high throughput sequencing. DNA

is commonly obtained from tissue homogenates consisting of a heterogeneous population of cells (typically thousands to millions). Therefore cells are essentially averaged together, regardless of cell type. There may be significant differences between cell types (ie. cardiomyocytes and fibroblasts) that are functionally important. When examining homogenates from tissues, various cell types within the tissue are treated as one sample in typical measurements. In doing so, potentially important cell-specific differences go unnoticed (Stålbert & Bengtsson, 2010). Novick and Weiner demonstrated the importance of single-cell analysis in the 1950's. They examined *Escherichia coli* and found that individual cells expressed β-galactosidase in an all-or-nothing phenomenon and that only the number of cells expressing β-galactosidase was changed, rather than a variation of β-galactosidase expression within single cells (Novick & Weiner, 1957). Another example of the importance of single-cell analysis is exemplified in cancerous fractional killing. Spencer et al. examined the effects of protein synthesis inhibitors on HeLa and non-transformed MCF-10A mammary epithelial cells. It was reported that differences in sister cell protein levels were initially similar but progressed to become so different that protein levels were eventually as dissimilar as two randomly chosen cells (Spencer et al., 2009). Importantly, the variation in gene expression led to individual cells producing varying concentrations of defense proteins that aided in protection against apoptotic death, and therefore some cells survived fractional killing while those that did not produce enough defensive proteins underwent apoptosis (Spencer et al., 2009). Interestingly, previous research has demonstrated that the aged mouse heart

displays elevated gene expression variation over time when compared to young mouse heart (Bahar et al., 2006).

Aging

Aging is commonly defined as a gradual loss of physiological function over time. This impaired function directly relates to an increased susceptibility to mortality. The aggregation of cellular damage is widely accepted as a general cause of aging (Gems and Partridge, 2013; Kirkwood, 2005; Vijg and Campisi, 2008). It is often difficult, however, to determine the sources of age-related damage, as well as the relationship between different types of damage and compensatory responses. For example, what is cause, versus compensation? Such considerations led Lopez-Otin to publish a review that has highlighted nine potential hallmarks of aging: genomic instability, telomere attrition, epigenetic alterations, loss of proteostasis, deregulated nutrient sensing, mitochondrial dysfunction, cellular senescence, stem cell exhaustion and altered intercellular communication (Lopez-Otin et al., 2013). This thesis will focus on two of the hallmarks of aging: mitochondrial dysfunction with an associated compensatory response.

One common theme of aging is the accumulation of genetic damage throughout life by endogenous factors, such as reactive oxidative species (Hoeijmakers, 2009; Moskalev et al., 2012). Mutations and deletions in aged mitochondrial DNA may play a significant role in aging (Park and Larsson, 2011). Mitochondrial DNA is suspected to be a major target for aging-associated

somatic mutations because of the oxidative microenvironment of the mitochondria, the lack of protective histones and the limited efficiency of the mtDNA repair mechanisms (Linnane et al., 1989). However, whether or not mtDNA mutations cause aging is controversial because cells contain more than one mitochondrial genome, and there have been a paucity of techniques available for determining single cells mutational load. Further confounding the difficulty in answering this question has been the potential for multiple different genomes within a single mitochondrion, in addition to multiple mitochondria within a cell. Coexistence of mutant and wild-type genomes is possible within the same cell, and this is termed “heteroplasmy.” Single-cell analysis has shown that the mutational load of individual aging cells becomes significant and may attain a state of homoplasmy in which one mutant genome is predominant (Khrapko et al., 1999), which likely arises due to a compensatory response within the cell.

Mitochondria contain their own genome, referred to as mitochondrial DNA (mtDNA). A long-standing theory of aging posits that the pathobiology of aging is due to the steady accrual of mutations in the mitochondrial genome due to the proximity to the production of reactive oxygen species as a normal function of cellular respiration. However, direct evidence for this “mtDNA theory of aging” has been difficult to experimentally test. This is due to the fact that the levels of mtDNA mutations are low when investigated at the “bulk” tissue level. Most investigations into the pathology and molecular biology of heart disease rely on homogenization of heart tissue, which combines and averages all the cell types in the heart together, including diverse cell types like fibroblasts, several types of

myocytes, and blood cells. This standard approach also does not take into account the potential variation between cells. Currently, there is little known with regard to potential variation of mtDNA copy number in individual cardiomyocytes, or whether or not mtDNA mutation accumulation varies in response to endogenous oxidative stress.

For many years, it has been proposed that oxidative stress within the mitochondria cause mutations to the mtDNA, which have been suggested to play a major role in the pathobiology of aging (Szczesny et al., 2003; Peuene et al., 2014). However, other studies report that impaired mtDNA repair mechanisms (mtDNA polymerase) play a larger role in mitochondrial-mediated disease (Ameur et al., 2011). In mtDNA disease, one of the first observable molecular hallmarks is the increase in mtDNA copy number per cell. However, with aging, evidence for this phenomenon is also somewhat controversial. The Melov laboratory has been developing a transgenic mouse model of mitochondrial oxidative stress in the heart, which is induced by constitutive inactivation of the reactive oxygen species detoxifying enzyme superoxide dismutase 2 (SOD2), located in the mitochondria. These mice experience oxidative stress and heart dysfunction. Therefore the *Sod2* knockout mice are an excellent model to test the hypothesis that endogenous oxidative stress can both cause an increase in mtDNA copy number per cell and cause an increased prevalence of mtDNA mutations. Importantly, oxidative stress can vary between individual cells; therefore, the overall goal of this project is to develop the methodology for isolating cardiomyocytes from *Sod2* null mice and to quantitate mitochondrial

copy number per cell. Ultimately, we hope to sequence the mtDNA per cell to determine if there is an increased burden of mtDNA mutations in single-cardiomyocytes compared to normal controls.

We hypothesized that constitutive *Sod2* knockout mice have cardiac dysfunction and contain less mitochondrial genomes per cell, accompanied by increased levels of mitochondrial DNA mutations, when compared to age-matched controls. In order to test this hypothesis, we carried out several experiments.

First, we confirmed the presence of cardiac dysfunction in constitutive *Sod2* knockout mice with echocardiography. *Sod2* knockout mice were previously reported to have pathology consistent with heart disease (Huang, et al., 2001; Koyama, et al., 2013). However, *in vivo* functional imaging had not been carried out. In order to verify that mice constitutively lacking *Sod2* have functional deficits of the heart, I acquired functional imaging of live *Sod2* null animals. This confirmed that key parameters of cardiac dysfunction, such as ejection fraction and fractional shortening, are altered in these mice.

Second, I developed a methodology for isolating specific ventricular cardiomyocytes from isolated regions of the neonatal mouse heart, which required optimization of prior protocols developed in the Melov lab. I first determined conditions for which viable cardiomyocytes could be liberated from extracellular matrix of dissected cardiac tissue, and I then developed methods for collecting individual single cells suitable for quantitative PCR.

Third, I developed a methodology for determining mitochondrial genome count in wild-type ventricular cardiomyocytes. Mitochondrial genome counts are a necessary first step prior to sequencing the mtDNA genome. In addition, we wished to determine if mtDNA copy number was altered between *Sod2* null mice versus controls. We determined that cardiomyocytes from mice undergoing endogenous oxidative stress had no more mitochondrial genomes, on average, than age-matched wild-type cardiomyocytes.

Lastly (although this is beyond the scope of this thesis), we will send single-cardiomyocytes to University of Minnesota to have the mitochondrial genomes sequenced. We will then compare the mutation rates between genomes from mice suffering from oxidative stress mediated heart disease against wild-type controls.

Materials and Methods:

Overview

All animal procedures will be in accordance with approved Institutional Animal Care and Use Committee protocols at the Buck Institute (American Association for Accreditation of Laboratory Animal Care accredited). CD-1 mice nullizygous for the *Sod2* locus (CD1-*Sod2*^{tm1Cje}) have been bred within the laboratory.

Genotyping

Each mouse used in this study was genotyped using the KAPA Mouse Genotyping Kit. Tail clips were obtained within the first day of life and immediately added to 2 µL of 1U/µL KAPA Express Enzyme, 10 µL of 10X KAPA Express Extract buffer, and 88 µL of PCR-grade water. The cells were lysed by incubation in the thermocycler for 10 minutes at 75℃. During this step the cells were lysed, nucleases and proteases were degraded and the DNA was released. The samples were then incubated for 5 minutes at 95℃ in order to inactivate the KAPA Express Extract protease. Samples were vortex for 3 seconds and centrifuged at a high speed for 1 minute in order to pellet debris. The DNA-containing supernatant (~70 µL) was transferred to a fresh tube. One µL of DNA extract was mixed with 25 µL of PCR master mix.

Table 1 - Genotyping Reaction: PCR

Master Mix:	Amount per reaction
PCR mix	10 µl
+/+ (w2) primer (0.2 mM) • 5'AAGAGCGACCTGAGTTGTAACA3'	0.1 µl
+/- (c2) primer (0.4 mM) • 5'CATCTAGTGGAGAAGTATAGTA3'	0.21 µl
-/- (m2) primer (0.4 mM) • 5'GCCTCGTTCATGAATATTCAGTT3'	0.21 µl
H_2O	5.48 µl

The neonatal lethal phenotype was prevented by 18 consecutive days of EUK-189 intraperitoneal injections at 10 mg/kg commencing at 3 days of age, consistent with prior studies (Melov et al., 1997, 2001). Methods for isolation of

cardiomyocytes utilized the protocol developed by the Melov lab and the Roepke lab (Flynn et al. 2011; Kohncke et al. 2013) and are described in detail, below, in the *cell isolation* section. Cardiomyocytes from both *Sod2* (+/+) (wild type) and *Sod2* (-/-) (knockout) have been isolated and frozen at -80 degrees Celsius.

Functional Echocardiography

Functional echocardiography measurements were evaluated in each mouse at 21 days old. The VisualSonics Vevo 2100 ultrasound system was used to measure the cardiac output, ejection fraction, and the stroke volume within the left ventricle. These metrics were obtained by observing the left ventricular long-axis and short-axis views, wall motion via m-mode, and mitral flow with Doppler pulse wave measurements.

Single-cardiomyocyte isolation

Each mouse was terminally sedated with an I.P. injection of sodium pentobarbital, rather than CO_2 affixation or cervical dislocation. The thoracic cavity was cut along the thoracic margin while the mouse was still breathing. The first incision was made along the abdominal wall, below the xiphoid process. The second and third incisions extend the original cut to both sides of the mouse, cutting the ribs in the medial axillary line. The rib cage was deflected upward, to expose the pericardium. While the heart was still beating, the aorta was clamped with forceps and all the connecting vessels were severed with a single cut.

The heart was immediately placed into a beaker containing ice-cold and pre-oxygenated solution A (see Table 2), and then transferred into a pre-warmed Petri dish containing low-calcium solution (Solution D). The aortic and other non-cardiac tissue were removed with scissors and discarded. The atria (left & right) and ventricles (left & right) were distinguished from one another and placed into separately labeled Petri dishes containing 5 mL of solution D.

Table 2 – Digestion buffer solutions (Köhncki et al., 2013)

Solution	Contents (in mM)
A	117 NaCl, 4 KCl, 10 HEPES, 1 KH_2PO_4, 4 $NaHCO_3$, 1.7 $MgCl_2$, 10 glucose
B	117 NaCl, 4 KCl, 10 HEPES, 1 KH_2PO_4, 4 $NaHCO_3$, 1.7 $MgCl_2$, 10 glucose + 229.5 µM EGTA
C	117 NaCl, 4 KCl, 10 HEPES, 1 KH_2PO_4, 4 $NaHCO_3$, 1.7 $MgCl_2$, 10 glucose + $CaCl_2$ 0.1 + 0.8 g/L collagenase type II
D	117 NaCl, 4 KCl, 10 HEPES, 1 KH_2PO_4, 4 $NaHCO_3$, 1.7 $MgCl_2$, 10 glucose + $CaCl_2$ 0.2 + 0.8 g/L collagenase type II + BSA (1 g/L)
E	117 NaCl, 4 KCl, 10 HEPES, 1 KH_2PO_4, 4 $NaHCO_3$, 1.7 $MgCl_2$, 10 glucose + $CaCl_2$ 0.5 + BSA (1 g/L)
F	117 NaCl, 4 KCl, 10 HEPES, 1 KH_2PO_4, 4 $NaHCO_3$, 1.7 $MgCl_2$, 10 glucose + $CaCl_2$ 1.0 + BSA (1 g/L)

In order to dissociate the cardiomyocytes from specific anatomical regions of the heart, the heart segments were gently pulled apart with fine forceps. A 1-mL pipette with an enlarged plastic tip was used to suspend the cells in 1 mL of solution E for 5 minutes, and the cells were separated from debris using a cell filter (200 µm mesh size). 5 mL of solution E was added to the cell suspension and centrifuged for 2 minutes at 16 x g at room temperature. The supernatant was discarded, and the pellet was re-suspended in 5 mL of solution F for 1 min

and then spun at 16 x g for 10 minutes. The resulting suspension was then allowed to settle for 10 minutes and centrifuged for an additional minute at 16 x g at room temperature. The supernatant was removed, and the pellet was resuspended into 3 mL of solution F.

In order to dissociate the ventricular cardiomyocytes, the heart segments were gently pulled apart with fine forceps. A 1-mL pipette with an enlarged plastic tip was used to suspend the cells in 1 mL of solution D for 5 minutes, and the cells were separated from debris using a cell filter (200 μm mesh size). 2.5 mL of solution D was added to the cell suspension and centrifuged for 2 minutes at 16 x g at room temperature. The supernatant was discarded, and the pellet was re-suspended in 5 mL of solution F at 16 x g for 10 minutes. The resulting suspension was allowed to settle for 10 minutes and subsequently centrifuged for one additional minute at 16 x g at room temperature. The supernatant was removed, and the pellet was re-suspended into 3.0 mL of solution F.

A micromanipulator was prepared by heating and shaping a glass capillary tube in order to pick single cardiomyocytes for nanofluidic PCR analysis. Viable cardiomyocytes made up about 70% of the filtered cell population. Healthy cardiomyocytes (displaying distinctive cardiomyocyte morphology) were selected under a dissection microscope, placed into individual PCR tubes, immediately frozen on dry ice, and then stored at -80°C.

Single-cell mitochondrial genome enumeration

Nanofluidic PCR was performed to assess single-cell mitochondrial genome count in cardiomyocytes of both wild-type and nullizygous *Sod2* mice. We used Fluidigm's nanofluidic PCR arrays (qd PCR 37K IFC) and Fluidigm's BioMark to determine the number of mitochondrial genomes present in each cardiomyocyte. Control line fluid was injected into each accumulator on the chip. The 48-well chip was placed into the IFC Controller MX, and we ran the Prime (167x) script to prime the control line fluid into the chip. The sample pre-mix and the final sample mixture were prepared as shown in Table 3 and were combined into a sterile tube in a DNA-free hood. 4.2 µL of the sample pre-mix was aliquoted for each sample (48 total). The aliquots were removed from the DNA-free hood, and 1.8 uL of DNA was added to each, making a total volume of 6 µL in each aliquot. When the Prime (167x) script had finished, the primed chip was removed from the IFC controller MX. 10 µL of 1X GE sample loading reagent was added to all hydration inlets. 4 µL of sample mix was added into the sample inlets on the chip, and the chip was returned to the IFC controller MX. The IFC controller MX software script (Load 167x) was run to load the samples into the chip. When the script was complete, the chip was removed from the IFC controller MX, and dust particles were removed from the chip surface. The chip was run within an hour of loading the samples. Data collection software, Digital PCR analysis software, and the calculating initial concentration equation were used to determine mitochondrial genome count for each cell (Figure 4).

Table 3 – BioMark Digital PCR Analysis Sample pre-mix

Component	Volume per inlet (μL)	Volume per inlet with overage (μL)	Volume per chip (μL)
TaqMan master mix (Applied Biosystems, PN 4369016)	2	3	180
20X GE Sample Loading Reagent (Fluidigm, PN 85000746)	0.4	0.6	36
20X gene-specific assays	0.2	0.3	18
DNA-free water	0.2	0.3	18
DNA	1.2	1.8	
Total	4	6	252

Figure 4 – Equation for determining mitochondrial genome count

$$\frac{\text{Estimated targets}}{\text{Panel}} \times \frac{\text{Panel}}{0.65\text{-}\mu\text{L}} \times \frac{4\text{-}\mu\text{L inlet}}{1.2\text{-}\mu\text{LDNA}} \times \text{Dilution factor} = \text{Initial copies/ } \mu\text{L}$$

Fig. 4. The *Initial Copies per μL Equation was* used to determine the mitochondrial genome count for each individual cardiomyocyte and fibroblast. Data from Fluidigm's Biomark was used to plug into the variables within this equation in order to determine mitochondrial genome count.

Masson's trichrome stain

Trichrome stains are used to study collagen fibers, muscle and connective tissue *in vitro.* A trichrome stain distinguishes collagen from muscle tissue. All reagents were prepared as described in the Sigma-Aldrich Accustain® Trichrome Stain (Masson) protocol (Procedure No. HT15).

First, 5-micron paraffin-embedded slides were deparaffinized in deionized water. Slides were left in Bouin's Solution (Catalog No. HT10-1) overnight at room temperature and then washed in running tap water. Slides were stained in

Working Weigert's Iron Hematoxylin Solution for 5 minutes, washed in running tap water for 5 minutes, and rinsed in deionized water. Slides were stained in Biebrich Scarlet-Acid Fucshin (Catalog No. HT15-1) for 5 minutes and rinsed in deionized water for 5 minutes. Slides were placed in Working Phosphotungstic/Phosphomolybdic Acid Solution for 5 minutes and then placed in Aniline Blue Solution (Catalog No. HT15-4) for 5 minutes. Slides were placed in 1% acetic acid for 2 minutes, dehydrated through ethanol, cleared in xylene and then mounted.

Western blot

The heart sample was placed in a weighing boat, and the weight was recorded. The heart was transferred into a mortar filled with liquid nitrogen and pulverized into a granular substance with a pestle. The granular substances were transferred into several different 1.5-mL Eppendorf tubes and stored at -80°C. The pulverized heart tissue was added to 300 µL of lysis buffer and allowed to sit on ice for 30-45 minutes to completely lyse the cells. A probe sonicator (setting 5-6 for 10 seconds) was used to break up membranes and tangles of DNA. Samples were spun for 2 min at 2,555 X g to remove any particulate, and the supernatant was transferred to a new tube and placed on ice. Protein standards were prepared for the assay using the Lowry Assay. Based upon the concentrations given by the Spectromax plate reader output data sheets, the amount of lysis buffer, protein, and LDS buffer needed to standardize all samples to 1 µg/µL was determined. Samples were prepared and stored at -20 degrees Celsius. 1X of Mes-SDS Running Buffer was prepared by adding 50 mL of 20X to

950 mL of nano-pure water. 1X TTBS solution was prepared by adding 50 mL of 20X TBS to 950 mL of nano-pure water and 1 mL of Tween. Blocking buffer was prepared by adding 1 gram of blocking reagent (dehydrated 2% milk) to 200-mL of 1X TTBS solution. 10 µL (equivalent of 10 µg of protein per lane) of standardized protein samples were loaded into the wells of a NuPage 4-12% Bis-Tris gel. Samples were initially run at low voltage (~60 V) for 20 min, and then the voltage was increased (~120 V) for about 40 minutes.

The proteins were then transferred onto a nitrocellulose membrane, and the sandwich was placed in the iBlot machine for 7 min at "P3" setting. The membrane was washed for 10 minutes in 25 mL of 1X TTBS and blocked for 1 hour. The membrane was incubated with primary antibody, diluted in blocking buffer solution to the concentration that the manufacturer recommended, overnight at 4 degrees Celsius. The membrane was washed four times with 25 mL of 1X TTBS for 5 min each and incubated with secondary antibody, diluted in blocking buffer solution to the concentration that the manufacturer recommended, for 1 hour at room temperature. The blot was washed four times with 20 mL1X TTBS for 5 minutes each. 1 mL of ECL was added evenly to the membrane, and the membrane was imaged with Alpha-Innotech Imager. Western blots were quantified using NIH's ImageJ program.

Statistical Analysis

Statistical analysis employing non-parametric analysis was used. The Melov lab uses a variety of statistical packages based on permutation testing in the statistical software R to test for significance. Permutation testing is the

method of choice, as it does not assume normality of the biological population from which one is sampling (Koch, 1966).

Future Studies:

mtDNA mutation detection

Single-cardiomyocytes will be sent to the University of Minnesota for next-generation sequencing. A primer sets have been designed (Figure 5) to completely cover the mitochondrial genome with overlaps. Once we obtain and analyze the sequence results, we will know all point mutations and deletions that occur in mice undergoing endogenous oxidative stress, and will be able to compare the effects of endogenous oxidative stress in the heart to wild type mice undergoing a lesser load of oxidative stress.

Figure 5 - Primer design for full mitochondrial genome coverage

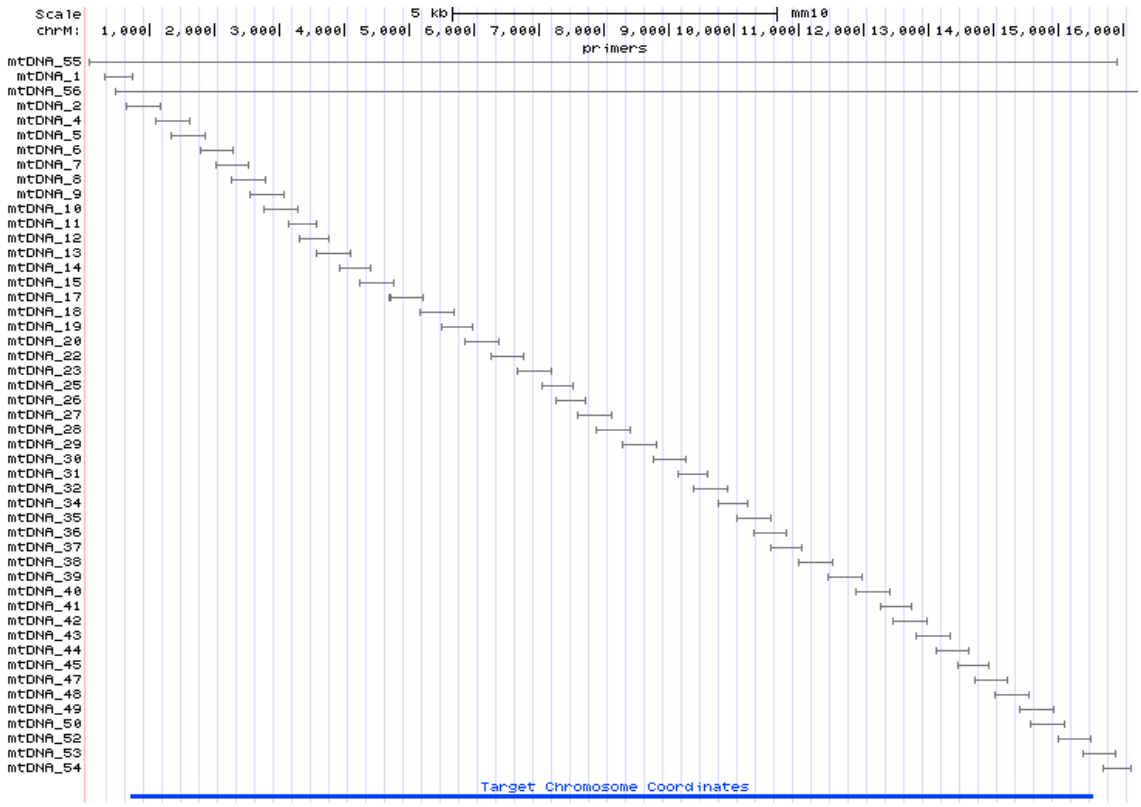

Fig.5. Custom designed primer sets that amplify PCR products for sequencing and covers the entire mitochondrial genome with overlaps. Any mutations that occur to the mitochondrial DNA, as a result of oxidative stress, will be detected by sequencing the genomes of *Sod2* nullizygous mice.

Results:

This study focuses on oxidative stress resulting in cardiac dysfunction. Echocardiography was used to assess the functionality of the heart undergoing endogenous oxidative stress in a similar way to a human clinical setting. The mice that contained only 1 PCR product at 500 bp were determined to be wild-type, while the mice with only 1 PCR product at 300 bp were determined to be *Sod2* knockout mice. *Sod2* knockout mice have a smaller PCR product because they do not contain a fully functional SOD2 enzyme. Heterozygous mice contain both PCR products, with 1 at 500 bp and 1 at 300 bp. All mice in this study were genotyped using PCR in order to confirm the knockout of the SOD2-encoding gene (Figure 6).

This was also confirmed at the protein level by using Western blot analysis. As expected, wild-type mice had SOD2 activity, while knockout mice did not have SOD2 activity (Figure 7). Body mass was also recorded in order to assess the health status of the animals in this study. Both the wild-type (*Sod2* +/+) and heterozygous (*Sod2* +/-) increased steadily in weight over the first three weeks of life, while the knockout mice (*Sod2* -/-) weighed less and began to lose weight after the second week of life (Figure 8).

Upon the third week of life, all mice were subjected to echocardiography. The Vevo 2100 software was utilized to obtain important heart metrics, such as ejection fraction (EF) and fractional shortening (FS). EF is the percentage of blood pumped out of the left ventricle during a cardiac cycle. The mathematical equation is defined as the stroke volume divided by the end diastolic volume.

Sod2 knockout (KO) mice have a significantly lower ejection fraction value than age-matched wild-type (WT) littermates (Figure 9). (N= 12, 4 knockouts and 8 wild type). Fractional shortening is the loss in left ventricular dimension between diastole and systole. This is calculated by the following mathematical equation:

[(LVED - LVES) / LVED] X 100.

Sod2 knockout mice had a significantly lower fractional shortening (FS) than age-matched wild-type littermates (Figure 9). (N= 12, 4 knockouts and 8 wild type). Importantly, these same metrics are used clinically and significantly decrease with age, hypertrophy, and cardiac fibrosis (Mizuguchi et al., 2010).

Masson's trichrome stain was performed to evaluate the level of cardiac fibrosis in *Sod2* KO mice and wild-type mice. *Sod2* knockout mice have more collagen type II secretion than wild-type mice as indicated by the blue stain interwoven between muscle fibers (Figure 10). Collagen type II secretion is indicative of cardiac fibrosis. Nuclei are stained black, cytoplasm and muscle fibers are red, and collagen is stained blue.

We were interested in understanding how various enzymes involved in oxidative phosphorylation are affected by oxidative stress. Aconitase levels were measured by Western blot in both heart and liver tissue. Liver tissue was examined in all Western blots because this tissue primarily uses glycolytic metabolism. Relative levels (obtained from the average of all wild-type samples) were unaffected by endogenous oxidative stress in the heart but were mildly decreased in the liver of the *Sod2* knockout mice (Figure 11). Aconitase is the enzyme that catalyses the isomerization of citrate into isocitrate, and therefore

plays a critical role in the citric acid cycle, which results in the production of NADH and is then processed during oxidative phosphorylation. This finding indicated that this enzyme involved in the citric acid cycle was not critically impaired in hearts undergoing endogenous oxidative stress.

We were also interested in understanding how oxidative stress affects the enzyme responsible for iron sulfur cluster assembly (ISCU). There was no significant difference in ISCU (Iron sulfur clustering assembly enzyme) levels between wild-type and *Sod2* nullizygous mice (Figure 12). ISCU acts as a scaffold for the assembly of iron-sulfur clusters. Iron-sulfur clusters are critical for the function of many DNA repair proteins and the regulation of iron levels. The double band present in the Western blot is due to a non-specific protein binding. Relative levels of ISCU within the heart and liver were unaltered when undergoing endogenous oxidative stress.

We also examined an enzyme known to contain an iron-sulfur group called ferrochelatase (FECH). FECH levels were significantly reduced in heart tissue of *Sod2* knockout mice, but not in liver tissue of KO mice (Figure 13). Ferrochelatase is an enzyme that catalyzes the last step in the biosynthesis of heme by inserting ferrous iron into protoporphyrin IX to generate heme. In humans, ferrochelatase deficiency is responsible for the manifestation of erythropoietic protoporphyria, a disease that results in the harmful accumulation of porphyrins.

Fluidigm's nanofluidic PCR arrays (qd PCR 37K IFC) and Fluidigm's BioMark were used to assess the number of mitochondrial genomes present in

each cardiomyocyte. (Figure 14 A., B., C.) Three Nanofluidic PCR runs were performed to assess single-cell mitochondrial genome count in cardiomyocytes of both wild-type and nullizygous *Sod2* mice. There was no significant difference in the number of mitochondrial genome copies between *Sod2* nullizygous and wild-type mice while using permutation testing to determine significance. (Figure 14 D.) Three types of fibroblasts (dermal, lung and embryonic) were also evaluated and, as expected, had significantly less mitochondrial genomes present in each individual cell compared to cardiomyocytes due differences in energy expenditure.

Dermal, lung, and embryonic fibroblasts all displayed low mitochondrial genome copy numbers due to their highly glycolytic metabolism (Figures 15 D, and 16). Cardiomyocytes contain many more mitochondrial genomes because of their reliance on oxidative phosphorylation (Figures 15 A, B, C and 16). Interestingly, oxidative stress does not affect mitochondrial genome copy number, as shown by no significant difference between *Sod2* knockout mice and wild-type mice ($P>0.2$). A wild-type pellet of cardiomyocytes was included to demonstrate the effectiveness of the isolation protocol developed in this study.

Figure 6 - Genotyping Results

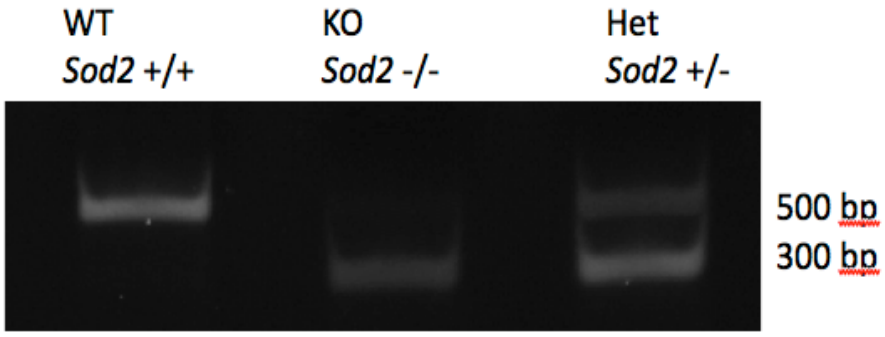

Fig.6. All mice in this study were genotyped to determine the status of the *Sod2* allele. Mice with only one PCR product at approximately 500 base pairs are confirmed wild type. Mice with two PCR products at 500 and 300 base pairs are heterozygous. Mice with one PCR product at 300 base pairs are confirmed *Sod2* null mice.

Figure 7 - SOD2 Western Blot

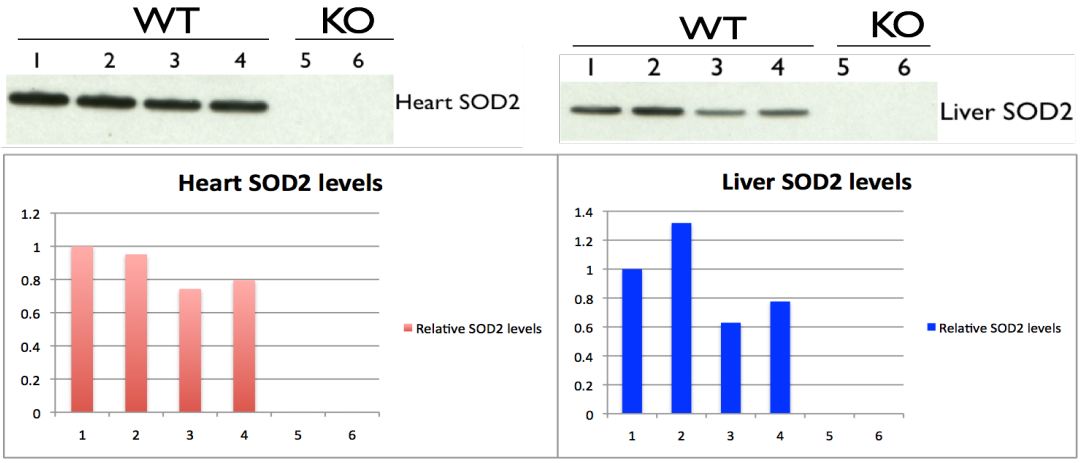

Fig.7 Anti-SOD2 antibody was used to confirm the presence/absence of SOD2. Wild-type levels of SOD2 are present in lanes 1-4, and *Sod2* knockout mice show a complete lack of SOD2 in lanes 5-6. Differences in SOD2 levels within lanes 1-4 may be due to differences in expression of the *Sod2* enzyme. Relative SOD2 levels were determined averaging the wild-type SOD2 levels.

Figure 8 - Weight Chart

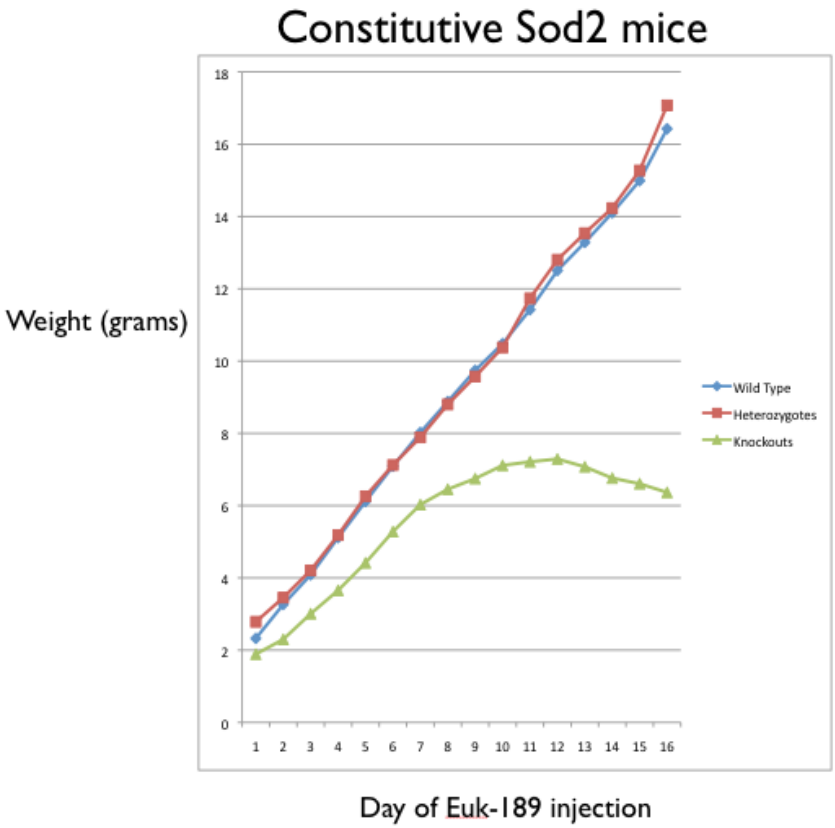

Fig.8. All 3-day-old mice were injected with Euk-189 until they were euthanized at 19-days-old. Wild type and heterozygous mice for the *Sod2* allele displayed a similar weight gain pattern during the first 3 weeks of development, while mice nullizygous for the *Sod2* allele weighed less overall and began to lose weight after about 2 weeks of age (N=40 for all groups, 10 for heterozygotes, 15 for wild-types, and 15 for *Sod2* null mice).

Figure 9 – Functional heart metrics

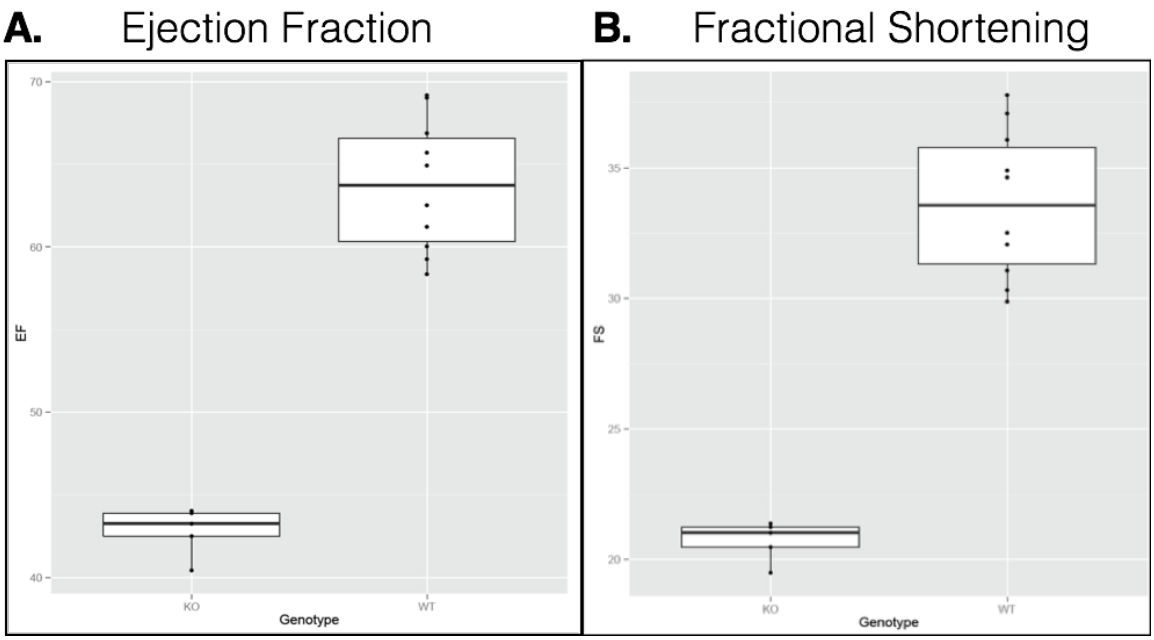

Fig.9. A. Ejection fraction is significantly lower in *Sod2* knockout (KO) mice when compared to wild-type (age-matched) controls (N= 12, 4 knockouts and 8 wild type). The middle horizontal bar represents the average value, the outer horizontal bars represent the standard deviation, and the vertical bars represent the variation within the sample. P<0.05 **B.** *Sod2* knockout mice had a significantly lower fractional shortening (FS) than wild-type (age-matched) littermates. (N= 12, 4 knockouts and 8 wild type). The middle horizontal bar represents the average value, the outer horizontal bars represent the standard deviation, and the vertical bars represent the variation within the sample. P<0.05

Figure 10 - Cardiac fibrosis

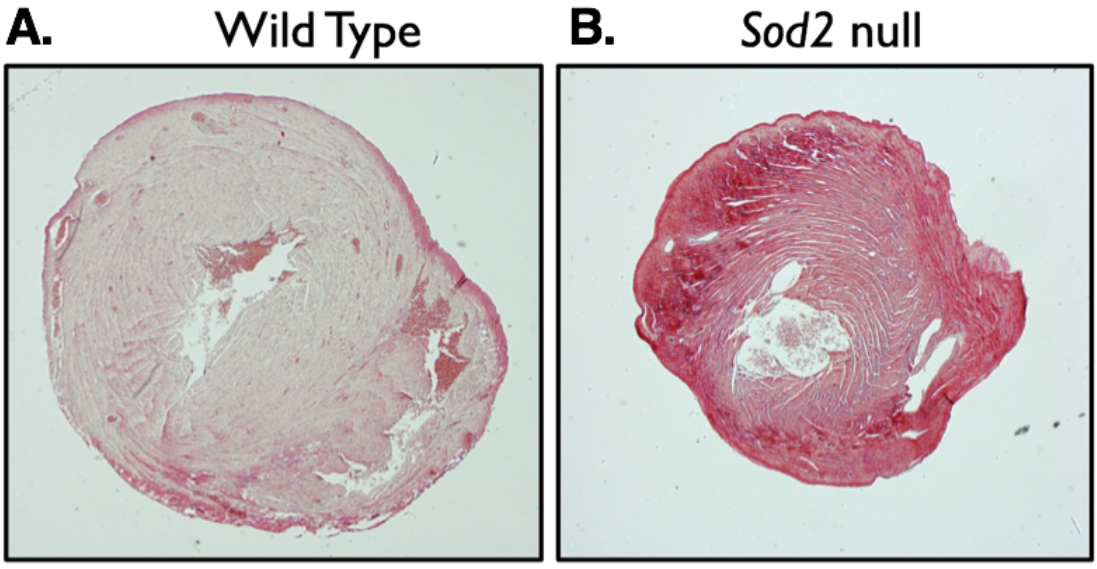

Fig.10. *Sod2* knockout mice have more collagen type II secretion than wild-type mice as indicated by the blue dye between muscle fibers. Collagen type II secretion is indicative of cardiac fibrosis. Nuclei are stained black, cytoplasm and muscle fibers are red, and collagen is stained blue.

Figure 11 - Aconitase activity

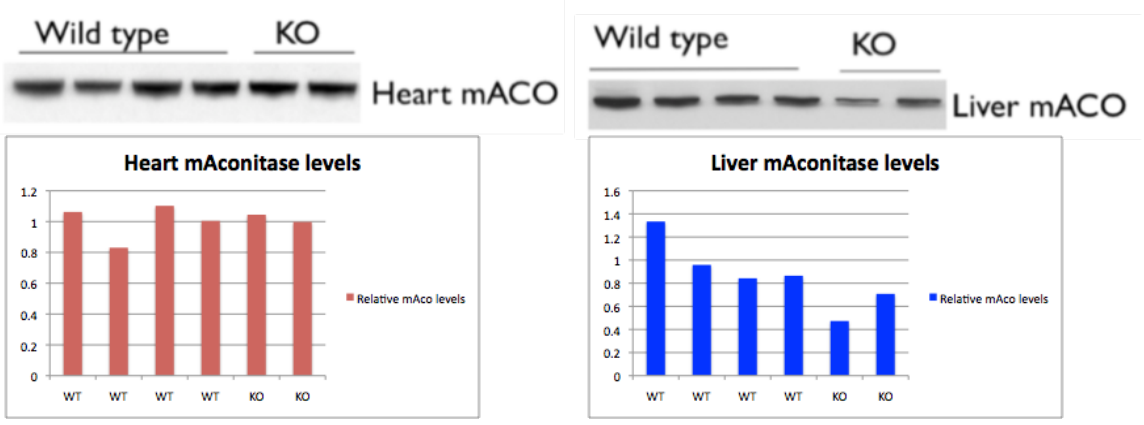

Fig.11. Aconitase levels were measured by Western blot, and relative levels were unaffected by endogenous oxidative stress in the heart but were mildly decreased in the liver of the *Sod2* knockout mice. Aconitase is the enzyme that catalyses the isomerization of citrate into isocitrate, and therefore plays a critical role in the citric acid cycle. This finding indicated that this enzyme involved in the citric acid cycle was not critically impaired in hearts undergoing endogenous oxidative stress (P>0.15). Relative aconitase levels were determined averaging the wild-type SOD2 levels.

Figure 12 - ISCU activity

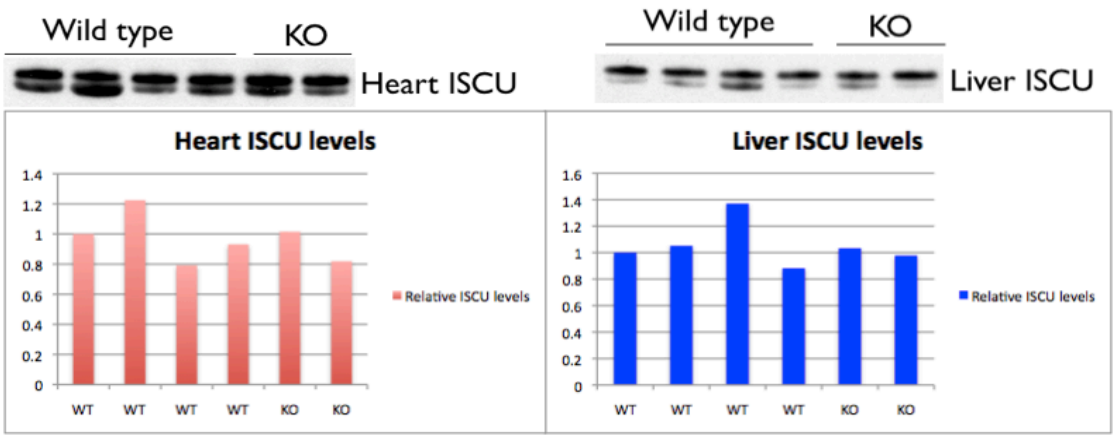

Fig.12. There was no significant difference ($p>0.1$) in ISCU (Iron sulfur clustering assembly enzyme) levels between wild-type and *Sod2* nullizygous mice. ISCU acts as a scaffold for the assembly of iron-sulfur clusters. Iron-sulfur clusters are critical for the function of many DNA repair proteins and the regulation of iron levels. Relative levels of ISCU within the heart and liver were unaltered when undergoing endogenous oxidative stress. The presence of the double band in the Western blot indicates non-specific binding of a protein that we believe to be hemoglobin due to its size. Relative SOD2 levels were determined averaging the wild-type SOD2 levels.

Figure 13 - Ferrochelatase activity

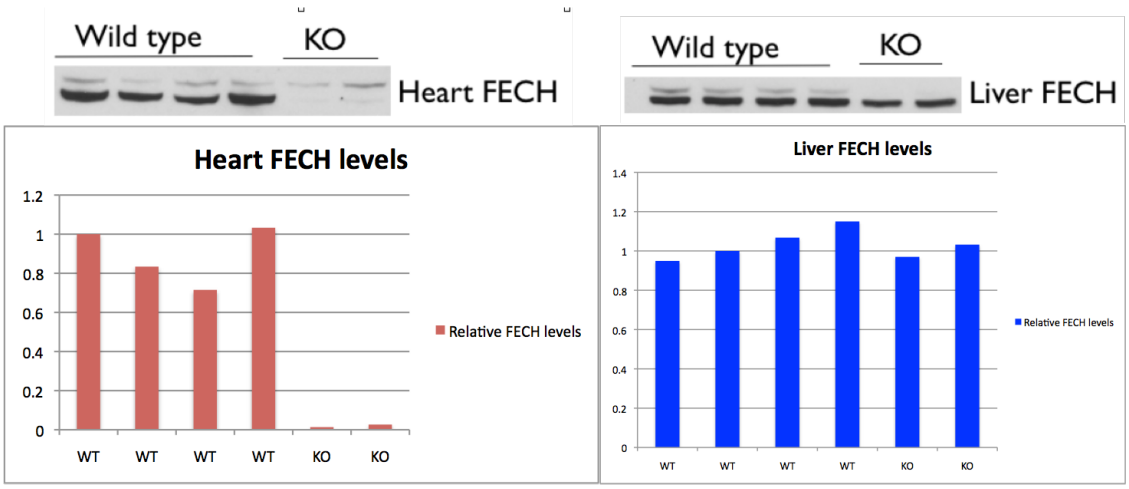

Fig.13. Ferrochelatase (FECH) levels were significantly reduced in heart tissue, but not in liver tissue of KO mice ($p<0.05$). Ferrochelatase is an enzyme that catalyses the last step in the biosynthesis of heme by inserting ferrous iron into protoporphyrin IX to generate heme. In humans, ferrochelatase deficiency is responsible for the manifestation of erythropoietic protoporphyria, a disease that results in the harmful accumulation of porphyrins.

Figure 14 – Single-cardiomyocyte mitochondrial genome enumeration

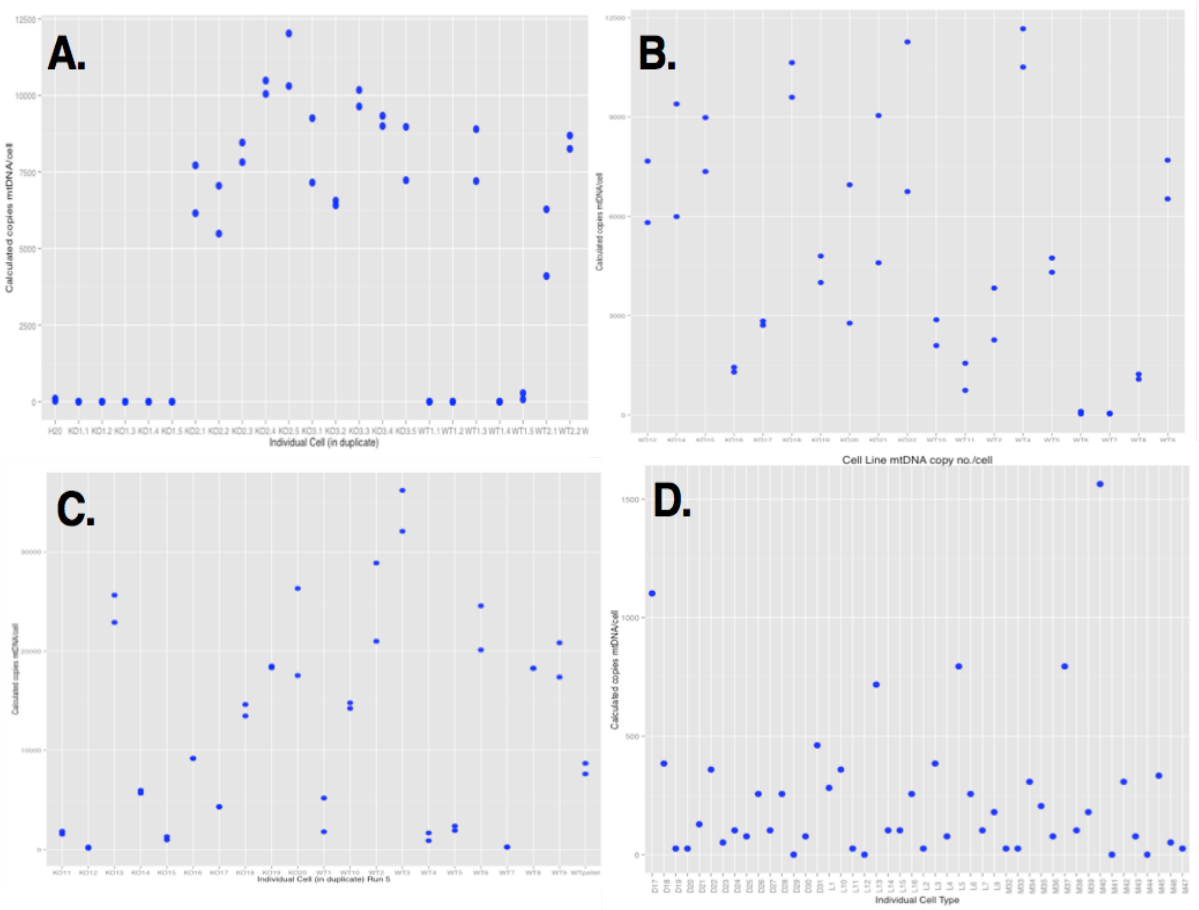

Fig.14. Fluidigm's nanofluidic PCR arrays (qd PCR 37K IFC) and Fluidigm's BioMark were used to assess the number of mitochondrial genomes present in each cardiomyocyte. (A-C) Three Nanofluidic PCR runs were performed to assess single-cell mitochondrial genome count in cardiomyocytes of both wild-type and knockout *Sod2* mice. There was no significant difference in the number of mitochondrial genome copies between *Sod2* knockout and wild-type mice. (D) Three types of fibroblasts (dermal, lung and embryonic) were also evaluated and, as expected, had significantly less mitochondrial genomes present in each individual cell compared to cardiomyocytes due differences in energy expenditure. Mitochondrial genome copy number displayed a high degree of variability cell-to-cell, with cardiomyocytes with as low as 38 mitochondrial genomes and cardiomyocytes as high as 34,142 mitochondrial genomes. This finding highlights the importance of performing single-cell analysis, rather than tissue homogenization. This variation in mitochondrial genome count would have gone unnoticed if tissue homogenization had been used.

Figure 15 – Mitochondrial genome enumeration summary

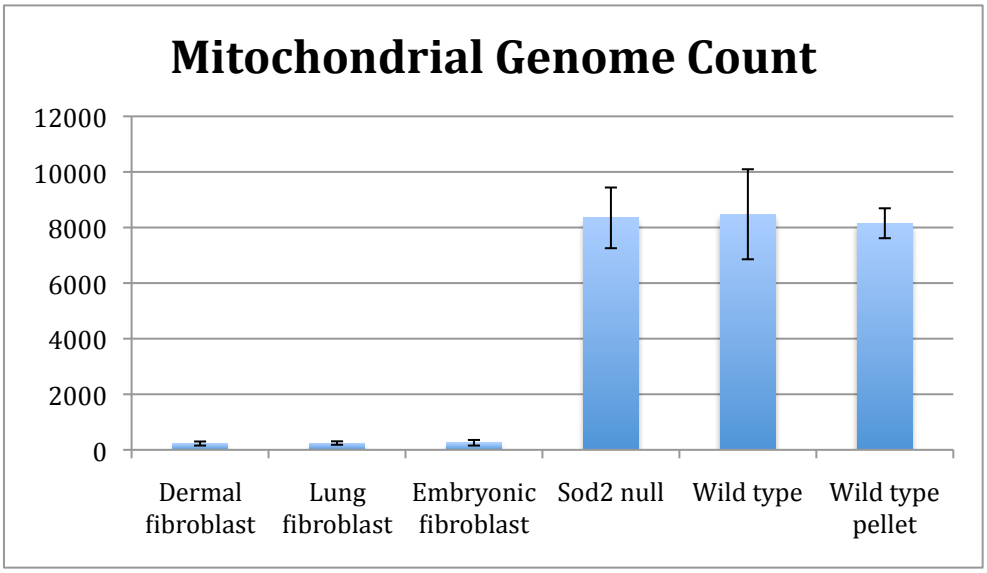

Fig. 15. Dermal, lung, and embryonic fibroblasts all displayed low mitochondrial genome copy numbers due to their highly glycolytic metabolism. Cardiomyocytes contain much more mitochondrial genomes because of their reliance on oxidative phosphorylation. Interestingly, oxidative stress does not affect mitochondrial genome copy number, as shown by no significant difference between *Sod2* knockout mice and wild-type mice (P>0.2). A wild-type pellet of cardiomyocytes was included to demonstrate the effectiveness of the isolation protocol developed in this study.

Discussion:

The purpose of this study was to determine the effects of oxidative stress on the heart of mice. We used a constitutive *Sod2* knockout model in order to induce oxidative stress. Echocardiography was used to assess cardiac dysfunction, a trichrome stain was performed to assess cardiac fibrosis, Western blotting was used to analyze enzyme activity involved in iron homeostasis and respiratory chain dysfunction, and single-cell analysis was utilized to quantitate mitochondrial genome count. Wild-type mice display values for ejection fraction (averaging 64%), whereas *Sod2* nullizygous mice have a significantly decreased ejection fraction (averaging 45%) within the left ventricle (Figure 9 A.). Ejection

fraction is calculated as stroke volume divided by end diastolic volume. Because the mice did not display a significant change in stroke volume compared to the wild type, it is reasonable to conclude that *Sod2* knockout mice undergo systolic dysfunction due to oxidative stress within the heart. In addition, *Sod2* nullizygous mice have a significantly lower fractional shortening value compared to wild-type mice (Figure 9 B.). This contributes to the theory that mice undergoing endogenous oxidative stress develop severely impaired systolic function.

Collagen accumulation, as shown in figure 10, is likely the result of the damage done to cardiomyocytes during such oxidative stress. Aconitase and ISCU levels were unaffected by endogenous oxidative stress (Figures 11 and 12), indicating that the damage associated with oxidative stress is not associated with the citric acid cycle nor the iron sulfur cluster scaffolding apparatus. Interestingly, FECH levels were significantly decreased in the heart, but not the liver, of mice undergoing oxidative stress (Figure 13). This suggests that oxidative stress may result in a lack of heme synthesis and an accumulation of porphyrins within the heart, and may result in the accumulation of pophyrins within heart and other tissues.

I developed a protocol for isolating ventricular cardiomyocytes from neonatal heart and contrasted copy number for the mtDNA genome within several dozen cells from *Sod2* nullizygous mice versus age-matched controls. Mitochondrial genome copy number displayed a high degree of variability cell-to-cell, with cardiomyocytes with as low as 38 mitochondrial genomes and cardiomyocytes as high as 34,142 mitochondrial genomes. This finding highlights

the importance of performing single-cell analysis, rather than tissue homogenization. This variation in mitochondrial genome count would have gone unnoticed if tissue homogenization had been used. If tissue homogenization alone was utilized, any cell-to-cell variation would have gone unnoticed, and this study emphasizes the importance of single-cell analysis.

Future Studies:

mtDNA mutation detection

Single-cardiomyocytes will be sent to the University of Minnesota for next-generation sequencing. A primer set has been designed to completely cover the mitochondrial genome with overlaps. Once we obtain results, we will gain insight into point mutations and deletions that occur in mice undergoing endogenous oxidative stress and will be able to compare this to sequencing results of single-cardiomyocytes from wild-type mice.

Gene expression profiling

Ferrochelatase activity is severely inhibited in mice undergoing oxidative stress. However, it is unclear what other enzymes are repressed in a tissue-specific manner, like FECH. As a result, gene expression profiling should be performed in order to determine differences in expression as a result of endogenous oxidative stress in the constitutive *Sod2* mouse model by using reverse transcriptase quantitative PCR.

References:

Ameur, A., Stewart, JB., Freyer, C., Hagström, E., Ingman, M., Larsson, NG., Gyllensten, U. (2011) Ultra-deep sequencing of mouse mitochondrial DNA: mutational patterns and their origins. *PLoS Genet.* 7(3):e1002028.

Bahar R., Hartmann C.H., Rodriguez K.A., Denny A.D., Busuttil R.A., Dollé M.E., Calder R.B., Chisholm G.B., Pollock B.H., Klein C.A., Vijg J. (2006) Increased cell-to-cell variation in gene expression in ageing mouse heart. *Nature* 441(7096) 1011-1014.

Bengtsson, M., Stahlberg, A., Rorsman, P., et al. (2005) Gene expression profiling in single cells from the pancreatic islets of Langerhans reveals lognormal distribution of mRNA levels. *Genome Res*. (15) 1388-1392.

Bergmann, O., Bhardwaj, R.J., Bernard, S., Zdunek, S., Barnabe-Heider, F., Walsh, S., Zupicich, J., Boveris, A. (1984) Determination of the production of superoxide radicals and hydrogen peroxide in mitochondria. *Methods in Enzymology* (105) 429–435.

Bracey, N.A., Beck, P.L., Muruve, D.A., Hirota, S.A., Guo, J., Jabagi, H., Wright, J.R., Macdonald, J.A., Lees-Miller, J.P., Roach, D., Semeniuk, L.M., Duff, H.J. (2013) The NIrp3 inflammasome promotes myocardial dysfunction in structural cardiomyopathy through interleukin-1β. *Exp. Physiology* 98 (2) 462-472.

Blomley, M.J., Cooke, J.C., Unger, E.C., Monaghan, M.J., Cosgrove, D.O. (2001) Microbubble contrast agents: a new era in ultrasound. *BMJ*. (322) 1222.

Crooks DR., Jeong, SY., Tong, WH., Ghosh, MC., Olivierre, H., Haller, RG., Rouault, TA. (2012) Tissue specificity of a human mitochondrial disease: differentiation-enhanced mis-splicing of the Fe-S scaffold gene ISCU renders patient cells more sensitive to oxidative stress in ISCU myopathy. *J Biol Chem.* 287 (48) 40119-30.

Doctrow S.R., Huffman K., Marcus, C.B., Tocco, G., Malfroy, E., Adinoli C.A., Kruk, H., Baker K., Lazarowich, N., Mascarenhas, J., Malfroy, B. (2002) Salen-manganese complexes as catalytic scanvengers of hydrogen peroxide and cytoprotective agents: structure-activity relationship studies. *J. Med. Chem.* 45 (20) 4549-4558.

Flynn, J.M., Melov, S. (2013) Endogenous oxidative stress in cardiomyocytes causes heart disease. In preparation.

Flynn, J.M., Santana, L.F., Melov, S. (2011) Single cell transcriptional profiling of adult mouse cardiomyocytes. *J. Vis. Exp.* (58).

Flynn, J.M., Spusta, S.C., Rosen, C., Melov, S. (2013) Single cell gene expression profiling of cortical osteoblast lineage cells. *Bone.* 53 (1) 174-181.

Gardin J.M., Arnold A.M., Bild D.E., et al. (1998) Left ventricular diastolic filling in the elderly: the cardiovascular health study. *Am J Cardiol* (82) 345-351.

Huang, TT., Carlson, EJ., Kozy, HM., Mantha, S., Goodman, SI., Ursell, PC., Epstein, CJ. (2001) Genetic modification of prenatal lethality and dilated cardiomyopathy in Mn superoxide dismutase mutant mice. Free Radic Biol Med. 31 (9) 1101-10.

Kitzman D., Sheikh K., Beere P., Philips J., Higginbotham M. (1991) Age-related changes of Doppler left ventricular filling indexes in normal subjects are independent of left ventricular mass, heart rate, contractility and loading conditions. *J Am Coll Cardiol* (18) 1243-1250.

Koch A.L. (1966) The logarithm in biology. I. Mechanisms generating the log-normal distribution exactly. *Journal of Theoretical Biology* (23) 276-290.

Kohncke, C., Lisewski, U., Schleuner, L., Gaertner, C., Rockert, S., Roepke, T.K. (2013) Isolation and kv channel recordings in murine atrial and ventricular cardiomyocytes. *J Vis Exp.* 12 (73).

Koyama, H., Nojiri, H., Kawakami, S., Sunagawa, T., Shirasawa, T., Shimizu, T. (2013) Antioxidants improve the phenotypes of dilated cardiomyopathy and muscle fatigue in mitochondrial superoxide dismutase-deficient mice. *Molecules* 8(2) 1383-93.

Li, Y., Huang, T.T., Carlson, E. J., Melov, S., Ursell, P. C., Olson, J. L., Noble, L.J., et al. (1995) Dilated cardiomyopathy and neonatal lethality in mutant mice lacking manganese superoxide dismutase. *Nature genetics* 11(4) 376–381.

Lloyd-Jones D.M., Larson M.G., Leip E.P., Beiser A,. D'Agostino R.B., Kannel W.B., Murabito J.M., Vasan R.S., Benjamin E.J., Levy D. (2002) Lifetime risk for developing congestive heart failure: the Framingham Heart Study. *Circulation (*106) 3068 –3072.

Melov, S., Doctrow, R., Schneider, J.A., Haberson, J., Patel, M., Coskun, P.E., Huffman, K., Wallace, D.C., Malfroy, B. (2001) Lifespan extension and rescue of spongiform encephalopathy in superoxide dismutase 2 nullizygous mice treated with superoxide dismutase-catalase mimetics. *J. Neurosci.* (21) 8348-8353.

Melov, S., Schneider, J.A., Day, B.J., Hinerfeld, D., Coskun, P., Mirra, S., Crapo, J.D., Wallace, D.C. (1998) A novel neurological phenotype in mice lacking mitochondrial manganese superoxide dismutase. *Nat Genet.* 18(2): 159-163.

Mezzaroma, E., E., Toldo, S., Farkas, D., Seropian, I.M., Van Tassell, B.M., Salloum, F.N., Kannan, H.R., Menna, A.C., Voelkel, N.F., Abbate, A. (2011) The inflammasome promotes adverse cardiac remodeling following acute myocardial infarction in the mouse. *Proc Natl Acad Sci USA* 108 (49) 19725-19730.

Mizuguchi, Y., Oishi, Y., Miyoshi, H., Luchi, A., Nagase, N., Oki, T. (2010) Concentric left ventricular hypertrophy brings deterioration of systolic longitudinal, circumferential, and radial myocardial deformation in hypertensive patients with preserved left ventricular pump function. *J Cardiol.* (1) 23-33.

Morten, K.J., Ackrell, B.A.C., and Melov, S. (2006) Mitochondrial reactive oxygen species in mice lacking superoxide dismutase 2: attenuation via antioxidant treatment. *The Journal of biological chemistry* 281(6) 3354–3359.

Novick, A., and Weiner, M. (1957) Enzyme induction as an all-or-none phenomenon. *Proc Natl Acad Sci USA* 15;43 (7) 553-566.

Puene, BN., Kimura, W., Muralidhar, SA., Moon, J., Amatruda, JF., Phelps, KL., Grinsfelder, D., Rothermel, BA., Chen, R., Garcia, JA., Santos, CX., Thet, S., Mori, E., Kinter, MT., Rindler, PM., Zacchigna, S., Mukherjee, S., Chen, DJ., Mahmoud, AI., Giacca, M., Rabinovitch, PS, Aroumougame, A., Shah, AMn Szweda, LA., Sadek, HA. (2014) The Oxygen-Rich Postnatal Environment Induces Cardiomyocyte Cell-Cycle Arrest through **DNA** Damage Response. *Cell* 157(3):565-79

Raha, S., Mceachern, G.E., Myint, A.T., and Robinson, B.H. (2000) Superoxides from mitochondrial complex III: the role of manganese superoxide dismutase. *Free Radical Biology Journal of Medicine* 29 (2) 170–180.

R Core Team (2012). R: A language and environment for statistical computing. R Foundation for Statistical Computing, Vienna, Austria. ISBN 3-900051-07-0, URL http://www.R-project.org/.

Szczesny, B., Hazra, TK., Papaconstantinou, J., Mitra, S., Boldogh, I. (2003) Age-dependent deficiency in import of mitochondrial DNA glycosylases required for repair of oxidatively damaged bases. *Proc Natl Acad Sci* 100(19) 10670-5.

Shioya, T. (2007) A simple technique for isolating healthy heart cells from mouse models. *Journal of Physiological Science* 57(6) 327–335.

Spencer, S.L., Gaudet, S., Albeck, J.G., Burke, J.M., & Sorger, P.K. (2009) Non-genetic origins of cell-to-cell variability in TRAIL-induced apoptosis. *Nature* 459 (7245) 428–432.

Ståhlberg, A., & Bengtsson, M. (2010) Single-cell gene expression profiling using reverse transcription quantitative real-time PCR. *Methods (San Diego, Calif.)* 50 (4) 282–288.

Sturtz, L.A., Diekert, K., Jensen, L.T., Lill, R., & Culotta, V.C. (2001) A fraction of yeast Cu,Zn-superoxide dismutase and its metallochaperone, CCS, localize to the intermembrane space of mitochondria. A physiological role for SOD1 in guarding against mitochondrial oxidative damage. *The Journal of biological chemistry* 276 (41) 38084–38089.

Szardien, S., Nef, H.M., Voss, S., Troidl, C., Liebetrau, C., Hoffmann, J., Rauch, M., Mayer, K., Kimmich, K., Rolf, A., Rixe, J., Troidl, K., Kojonazarov, B., Schermuly, R.T., Kostin, S., Elsaaser, A., Hamm, C.W. Mollmann, H. (2011) Regression of cardiac hypertrophy by granulocyte colony-stimulating factor-stimulated interleukin-1β synthesis. *Eur Heart J* 33 (5) 595-605.

Turrens, J.F., and Boveris, A. (1980) Generation of superoxide anion by the NADH dehydrogenase of bovine heart mitochondria. *The Journal of biological chemistry* 191 (2) 421–427.

Winter, R., Jussila, R., Nowak, J., Brodin, L.A. (2007) Speckle tracking echocardiography is a sensitive tool for detection of myocardial ischemia: A pilot study from the catheterization laboratory during percutaneous coronary intervention. *J Am Soc Echocardiogr* (20) 974-981.

Zhou, R.H., Vendrov, A.E., Tchivilev, I., Tchivilev, I., Niu, X.L., Moinar, K.C., Rojas, M., Carter, J.D., Tong, H., Stouffer, G.A., Mandamanchi, N.R., Runge, M.S. Mitochondrial oxidative stress in aortic stiffening with age: the role of smooth muscle cell function. *Atherioscler Thromb Vasc Biol* 32 (3) 745-755.